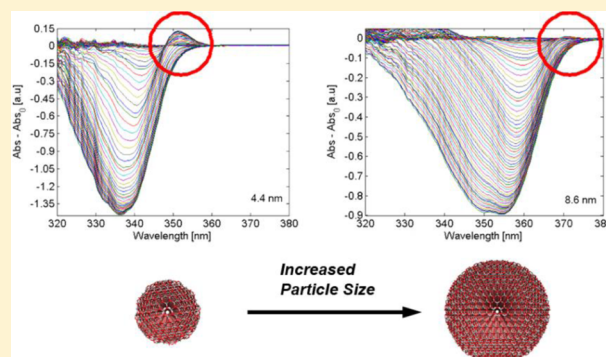# Quantum Confined Stark Effects in ZnO Quantum Dots Investigated with Photoelectrochemical Methods

T. Jesper Jacobsson and Tomas Edvinsson*

Department of Chemistry—Ångström Laboratory, Uppsala University, Box 538, 75121 Uppsala, Sweden

S *Supporting Information*

ABSTRACT: The optical absorption behavior of ZnO quantum dots has been investigated as a function of particle size in the quantum confined regime, between 4 and 9 nm in diameter, by using photoelectrochemical methods. Thin films of quantum dots, with 18 different sizes, were prepared on conducting substrates where the Fermi level could be controlled potentiostatically simultaneously as absorption measurements were performed. While raising the Fermi level into the conduction band, the dominant effect is a decrease in absorption as a consequence of increased electron population in the conduction band. This is a potentiostatic analogue to the Burstein—Moss shift for degenerate semiconductors. For applied potentials in an interval of 0.2 eV below the conduction band edge, the absorption does, however, increases instead of decreases. This absorption increase was found to be caused by a transition into states located within the band gap, which are introduced as a consequence of the applied potential. The magnitude of this effect is for the smallest particles (4 nm) approximately 9% compared to the magnitude of the Burstein—Moss bleaching. The effect decreases with increased particle size and essentially disappears for particles approaching 9 nm. The phenomenon is analyzed in terms of the Stark effect where the consequence of the applied potential is a buildup of an electric field within the particles, breaking the symmetry and splitting the energy levels in the conduction band. The gradual disappearance of the effect for the growing particles gives the extent of the quantum confinement effects of this phenomenon. The size-dependent absorption probability is analyzed and gives important information concerning the nature of both the perturbed states above the conduction band edge and the formation of the sub-band edge states.

1. INTRODUCTION

Zinc oxide, ZnO, is an interesting material with applications spanning from the simple and well-known to the highly advanced and sophisticated. Its wide band gap and high absorptivity have made it useful as UV-absorbing additive in everything from sunscreens,[1] advanced plastics,[2] and rubber.[3] It is also used in pigments[4] and food additives.[5] Besides these conventional applications, ZnO, and especially various nano-scale morphologies, have emerged as promising candidates for a large set of new high-tech applications. Among these are UV lasers,[6] light-emitting diodes,[7] field emitters,[8] piezoelectric devices,[9] spintronic devices,[10] gas sensors,[11] transparent conductors,[12] self-powered nanosystems,[13] photovoltaics,[14] and photocatalysis,[15] to mention just a few.

Several of these nanoscale applications are based on controlling the optical properties. In order to properly understand these and in order to control them, a greater knowledge is needed concerning the position, nature, and relation between all the energy states in the material affecting the optical behavior. This is especially true for small ZnO nanoparticles where the properties of the states will be a function of particle size and to some extent also on the preparation condition.

We have in a number of previous papers experimentally investigated how the band gap,[16] the band edge positions,[17] and the energy levels important for the fluorescence[18] depend on particle size for ZnO quantum dots in the regime of optical quantum confinement below 9 nm in diameter. In this paper, we explore and describe a second-order absorption gain in thin films of ZnO quantum dots, found under potentiostatic control of the Fermi level. The phenomenon is investigated for films with 18 different particle sizes, ranging from 4.4 to 8.6 nm in diameter.

The Fermi level in the ZnO particles can be experimentally controlled by placing an electrode with a thin film of particles in an electrolyte, connected in a three-electrode configuration, and scanning the potential. When a negative potential is applied, the Fermi level in the particles rises and is eventually negative enough for the Fermi level to reach above the conduction band edge. These states will then be occupied by electrons from the potentiostat. This will prevent excitation of electrons up to these states, resulting in a decreased absorption as well as an

increase in the optical band gap. This is a potentiostatic analogue to the Burstein−Moss effect for degenerate semiconductors. The effect can, if combined with absorption measurements, be used for extracting the absolute energetic position of the band edges, which was done as a function of particle size in a previous study.[17]

In this paper, a second-order absorption effect is investigated. In an interval of applied potentials, where the Fermi level is below the conduction band edge, the absorption for light with lower energy than the band gap increases. This effect is seen before the absorption bleaching due to the potential analogue of the Burstein−Moss effect and demonstrates that a more detailed picture is needed for understanding the electro-optical behavior of these particles. The magnitude of this effect is dependent on the particle size and decreases for larger particles. We propose an explanation for these phenomena in terms of the quantum confined Stark effect effective just before the effect of the Burstein−Moss shift starts to dominate. In particular, the size-dependent optical properties, both to the states above the conduction band edge and to the states induced by the local field, give information on both the extension of local field and its effect on the orbitals and optical properties in low-dimensional ZnO. The paper starts with a short derivation of the important factors in the absorption coefficient and a description of the dominant effect of the Burstein−Moss bleaching. The article continues with a description of the experiments and a detailed description of the experimental findings. In the end of the article, the phenomenon is discussed and analyzed in terms of the quantum confined Stark effect.

2. THEORY

In order to analyze the optical properties and the electronic transitions into states in the conduction band and into the induced states in the band gap, it is valuable to analyze the derivation of the expressions for the absorption coefficient in a direct semiconductor. This is important since it illuminates the different approximations applied in the derivation as well as identifying the main components affecting the absorption coefficient. In a semiconductor crystal, the electrons will experience a periodic potential which motivates the replacement of the ordinary wave function with Bloch functions, which eigenvalues are the band structure energies, $E_n(k)$, in reciprocal space. By considering the primitive cell in the reciprocal space, i.e. the Brillouin zone (BZ), and the initial and final bands as the valence band energy, $E_v(\mathbf{k})$, and the conduction band edge, $E_c(\mathbf{k})$, the Fermi golden rule for a crystal can be formulated as eq 1[19,20]

$$T_{v\to c} = \frac{2\pi}{\hbar} \int_{BZ} \frac{1}{4\pi^3} |H'_{vc}|^2 \delta(E_c(\mathbf{k}) - E_v(\mathbf{k}) - \hbar\omega) \, d\mathbf{k}$$

(1)

where $T_{v\to c}$ is the transition probability between the valence band (v) and the conduction band (c) for a wavelength corresponding to the energy $\hbar\omega$. The integral in eq 1 is performed over the Brillouin zone with the normalization $1/4\pi^3$ coming from the $2/\Omega$ number of spin states per unit volume, $8\pi^3/\Omega$ of the primitive lattice cell. For a direct transition, where there is no change in the crystal momentum between the initial, k_i, and final states, k_f, the initial and final energies are k-independent. For UV and visible light, the perturbation matrix element can be considered independent of the k-vector within the BZ as the wavelength of the perturbing light is much larger than the dimensions of the interaction volume.[20] The

perturbation matrix element, $|H'_{vc}|^2$, can thus be taken outside the integral in eq 1. Using the effective mass approximation and some exercise in mathematics (see Supporting Information), the functional form of the Fermi golden rule in a crystal with a direct band gap can be written as eq 2.

$$T_{v\to c} = \frac{2\pi}{\hbar} |H'_{vc}|^2 g_{cv}(\hbar\omega) = |H'_{vc}|^2 \frac{1}{\hbar\pi} \left(\frac{2m^*_{red}}{\hbar^2}\right)^{3/2}$$
$$\times (\hbar\omega - E_g)^{1/2}$$

(2)

where g_{cv} is the joint density of states between the conduction band and the valence band, m^*_{red} is the reduced effective mass, and E_g is the optical band gap. The perturbation Hamiltonian, H'_{vc}, can in turn be expressed in terms of how the incoming spatial electromagnetic field, $\mathbf{A}(\mathbf{r})$, induces a displacement of the electron and thus in terms of the transition dipole moment, μ_{vc}, as in eq 3

$$H'_{vc} = -\frac{i\omega\mathbf{A}}{m_0} \int \psi_v^* e\mathbf{r}\psi_c \, d^3\mathbf{r} = -\frac{1}{m_0}\boldsymbol{\mu}'_{vc}\cdot\mathbf{E}_0$$

(3)

where ψ_v^* is the complex conjugate of the crystal orbital wave function of the valence band, ψ_c is the crystal orbital wave function of the conduction band, e is the elementary charge of an electron, and $\mathbf{r}$ is the displacement. Since the expectation value of the displacement for a small interaction volume is small compared to the wavelength, eq 3 can in the last part utilize the dipole approximation and thus the assumption of the independence of the spatial field $\mathbf{A}(\mathbf{r})$ for a small displacement $\mathbf{r}$. For a given direction of the polarization field, $\mathbf{E}_0$, and an effective mass of the electron in the valence band, m_v^*, valid in the quadratic field, the transition probability can be expressed in terms of the scalar dipole and the magnitude of the field, which gives eq 4 for the transition probability for an electron in the valence band to be excited into the conduction band.

$$T_{v\to c} = \frac{E_0^2\mu_{vc}^2}{\hbar\pi m_v^*} \left(\frac{2m^*_{red}}{\hbar^2}\right)^{3/2} (\hbar\omega - E_g)^{1/2}$$

(4)

The absorption coefficient, $\alpha(\hbar\omega)$, is defined as the energy absorbed per unit time and unit volume, divided by the incoming energy flux in the media. An analytical expression for the absorption coefficient of direct semiconductors were first stated in a paper by Hall et al.[19], and citations for the first derivation are commonly referring to the same authors in a conference proceeding.[21] Interesting to note is that the derivation for a direct semiconductor is not found in either of these references but instead found in Fan et al. in the same proceeding[22] and also in a review article the same year.[23] The expression, as well as some slightly different forms of the expression, can also be found in Brooks et al.[24] and by Moss.[25] The expression given in eq 5, where e is the electron charge, c is the speed of light, n is the refractive index, and h is Planck's constant, can be found in other places, like for example in the commonly used Pankovés optical processes in semiconductors,[26] which refer back to the article by Hall et al.

$$\alpha(h\omega) \approx \frac{e^2}{nc}\frac{1}{h^2 m_n^*}(2m^*_{red})^{3/2}(h\nu - E_g)^{1/2}$$

(5)

The different forms of the expression found in the literature and the, in many places, unclear assumptions in arriving at the

final expressions motivate a short derivation of the absorption coefficient.

We can start by defining the incoming energy flux, S, via the Poynting vector,[27] $\mathbf{S}(\mathbf{r},t) = \mathbf{E}(\mathbf{r},t) \times \mathbf{H}(\mathbf{r},t)$ where the electric, E, and magnetic, H, field can be expressed in terms of the vector potential of the incoming light, $\mathbf{A}$. Choosing $\nabla \cdot \mathbf{A} = 0$ and thus the Lorentz gauge and setting the background scalar potential to zero, the incoming electromagnetic field can be described as $\mathbf{A}(\mathbf{r},t) = E_0 e^{i \cdot (\mathbf{k} - \omega t)}$, where the wave vector k is defined as $k^2 = \varepsilon_0 \mu_0 \omega^2$. Specifying the Poynting flux and utilizing time-averaging (see Supporting Information), the electromagnetic flux is given by $\langle \mathbf{S}(\mathbf{r},t) \rangle = (\omega E_0^2/2 \, \mu) \hat{k}$ with the magnitude

$$|\langle \mathbf{S}(\mathbf{r},t) \rangle| = \frac{\omega E_0^2}{2\mu} \hat{k} = \frac{\omega^2 E_0^2 n}{2\mu c} = n c \varepsilon_0 \frac{\omega^2 E_0^2}{2} \qquad (6)$$

where n is the refractive index of the material, c is the speed of light, and the magnetic permeability, $\mu = \mu_0$, can be taken as unity for nonmagnetic materials. The absorption coefficient for the first electron in the valence band can now be written as the rate transition of electrons, given by eq 4, divided by the number of photons per second, given from the optical electric field in eq 6, and can be written as eq 7

$$\alpha(\hbar\omega) = \frac{T_{v \rightarrow c}}{S/\hbar\omega} = \frac{E_0^2 \mu_{vc}^2 2\hbar\omega}{\hbar \pi m_v^* n c \varepsilon_0 \omega^2 E_0^2} \left(\frac{2m_{red}^*}{\hbar^2} \right)^{3/2}$$

$$\times (\hbar\omega - E_g)^{1/2} = \frac{2\mu_{vc}^2}{\pi m_v^* n c \varepsilon_0 \omega} \left(\frac{2m_{red}^*}{\hbar^2} \right)^{3/2} (\hbar\omega - E_g)^{1/2} \qquad (7)$$

where the dependence of the magnitude of the electric field has been canceled as the absorption should be independent of light intensity in the linear region. The derivation above illuminates that the nature of the assumed light, as well as the choice of radiation gauge, will naturally affect the prefactor in the expression for the absorption coefficient. In the present derivation, it could be noticed that there is a dependence on the effective mass in the valence band instead of a general effective mass of the electron, as in eq 5. Equation 7 also has a retained dependence on the transition dipole moment, $\mu_{v c}$, that is approximated away in eq 5 and is one of the important factors addressed in the Results and Discussion section.

In a degenerate semiconductor, the doping can reach such a level that the Fermi level no longer is located within the band gap. For an n-type semiconductor, the Fermi level will then reside within the conduction band. This results in a lack of empty states close above the band edge to which electrons can be excited. The absorption will therefore decrease, and the optical band gap will increase. This effect is commonly denoted as a Burstein−Moss shift, after work by Burstein[28] and Moss.[29] A sketch of this concept is given in Figure 1. Simple geometry[17] gives, under the assumption of parabolic bands close to the band edges, a relation between the intrinsic band gap, E_g, and the optical band gap, E_{opt}, given in eq 8

$$E_{opt} = E_g + \left(1 + \frac{m_n^*}{m_p^*} \right) (E_f - E_{cb} - 4k_B T)$$

$$\text{while } E_f > E_{cb} \qquad (8)$$

where E_f is the energy at the Fermi level, E_{cb} the energy at the conduction band, T is temperature, and k_B is Boltzmann's constant. This effect does not necessarily depend on the
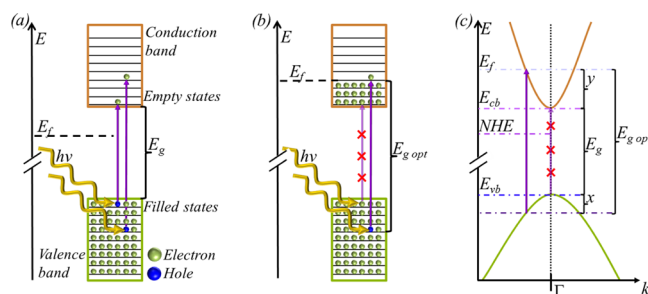

Figure 1. (a) Absorption in the undisturbed case where an electron in the valence band is excited to an empty level in the conduction band. (b) The situation under a negative applied potential where the Fermi level is located within the conduction band, illustrating how the optical band gap is increased under these conditions. (c) The relevant energy levels in (a) and (b) within the parabolic approximation.

concept of degeneracy by doping but could also be achieved electrochemically. This is based on the fact that the potential applied by the potentiostat, under steady-state conditions, to a good approximation will equal the Fermi level in the material. By applying a negative potential with the potentiostat, the Fermi level will rise, and for a potential negative enough, the Fermi level will reach the conduction band.

Given that there are counterions in the electrolyte, capable of balance extra charge within the semiconductor, empty states within the conduction band can then be filled from the potentiostat, thereby increasing the optical band gap. Using a three-electrode setup and measuring the absorption under a potential scan, the observed decrease in absorption can, together with eq 8, be used for extracting information on the absolute position of the band edges. This was done in a previous study[17] for these particles where also the kinetic conditions for the steady-state filling of the states were quantified. The absorption decrease while applying a negative potential is the dominant effect, but it is not the only effect present as demonstrated in this work.

3. EXPERIMENTS

3.1. Synthesis. ZnO nanoparticles were synthesized by a wet chemical method described in detail before[16] and are originally based on earlier works from Meulekamp[30] and Spanhel et al.[31] In the synthesis, one solution is prepared by dissolving 2.5 mmol of $Zn(OAc)_2 \cdot 2H_2O$ in boiling ethanol. Another solution is simultaneously prepared by dissolving 3.5 mmol of $LiOH \cdot H_2O$ in 25 mL of ethanol. When the two solutions are mixed, ZnO quantum dots begin to nucleate and grow in the solution. The growth can be monitored by following the decrease in optical band gap using UV−vis spectroscopy.[16]

At certain times, a small volume of the reaction solution was used for depositing thin films of particles with distinct sizes. This was done by mixing 2.5 mL of the reaction solution with approximately 5 mL of hexane. This decreases the particle solubility and leads to agglomeration and precipitation. The solution was then centrifuge at 5000 rpm for 5 min to speed up the sedimentation, and the particles were then redispersed in one drop of methanol and ultrasonicated for 3 min. The concentrated particle solution was then doctor bladed on substrates of conductive glass, whereupon smooth and transparent films were formed. Fluorine-doped SnO_2 (FTO) Pilkington TEC 8 was used as a conducting substrate in order
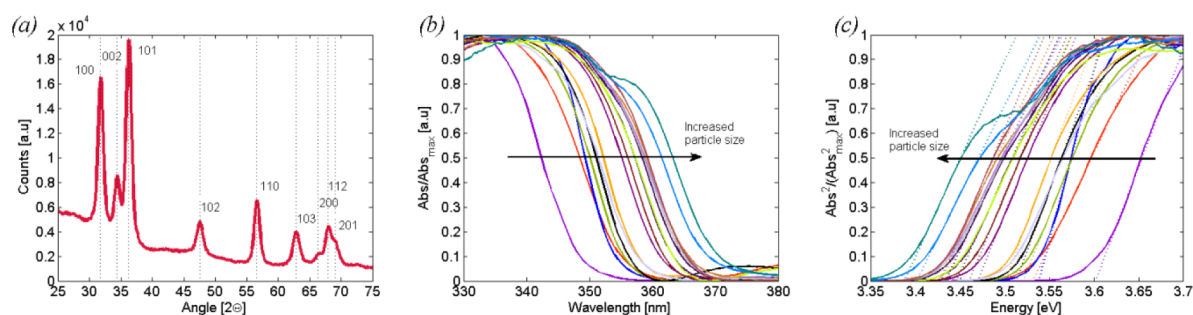
Figure 2. (a) XRD data for a representative sample of some of the largest particle, together with literature data for ZnO wurtzite. (b) Normalized absorption data for the analyzed samples. (c) Determination of the band gap as the intercept between the photon energy and the extrapolation of the linear region of the square of the absorption.
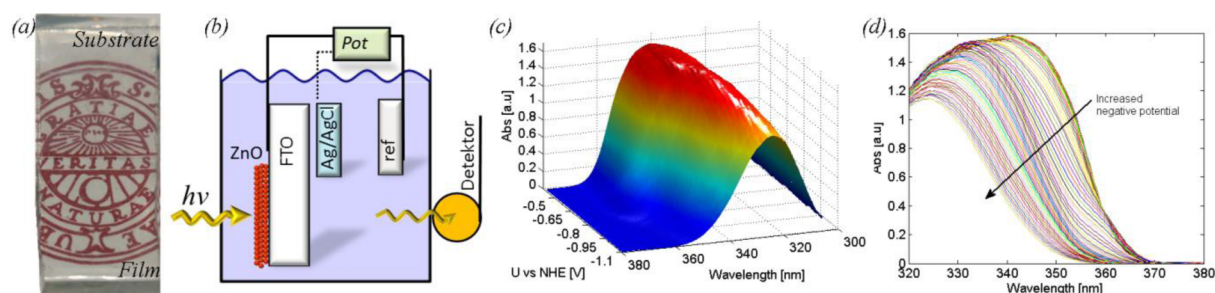

Figure 3. (a) A photo of a typical ZnO particle film on FTO. The film is on the lower part of the substrate and is slightly antireflective. (b) A sketch of the experimental setup. (c) Absorption as a function of wavelength and applied potential for a representative sample with 6.2 nm particles. (d) The two-dimensional projection of (c).

to enable combined electrochemical and transient absorption measurements.

3.2. Measurements and Characterization. UV−vis absorption measurements were performed with an Ocean Optics spectrophotometer, HR2000+, with deuterium and halogen lamps. In all measurements, a full spectrum from 190 to 1100 nm with 2048 evenly distributed points was sampled, and in order to obtain good statistics, an over 100 consecutive spectra were done.

The electrochemical measurements were performed with a CHI potentiostat 760. Potentials were measured against an Ag/AgCl reference electrode shifted 0.197 V with respect to the normal hydrogen electrode (NHE). A platinum wire was used as a counter electrode, and 0.5 M Na_2SO_4 was used as electrolyte.

Potential-dependent absorption was measured on the particle films in a three-electrode setup by scanning the potential from −0.3 V down to −1.3 V vs Ag/AgCl, simultaneously as the UV−vis absorption was measured perpendicular to the film. The scan rate was chosen sufficiently low to ensure steady state with respect to the absorption behavior at every potential. A scan rate of 10 mV/s was found to be appropriate for this. Absorption data were recorded once a second during the potential sweep. The potential interval was chosen wide enough to capture the behavior under study but still small enough to prevent corrosion of the electrodes in the time frame of the measurements.

XRD measurements were performed with a Siemens D5000 diffractometer using parallel beam geometry, an X-ray mirror, and a parallel plate collimator of 0.4°. Cu Kα with a wavelength of 1.54 Å was used as X-ray source. The angle of incidence was 0.5°, and 2Θ scans were performed between 10° and 90°, using a step size of 0.1°.

4. RESULTS AND DISCUSSION

X-ray diffraction for a representative sample of one of the quantum dot films is given in Figure 2a. Data are given together with literature values for the peak positions of wurtzite ZnO,[32] which is the only crystalline phase present in the films. The experimental XRD peaks are rather broad as a consequence of the small size of the particles.

The properties of these particles have been investigated quite extensively in a number of papers. Special focus has been given to size-dependent properties of the absorption,[16] fluorescence,[16,18] phonon behavior,[33] photocatalytic activity,[15] and the electrochemical properties.[15,17] For a more in-depth discussion on material characterization for these particles, the reader is referred to these articles.

For this particular investigation, 18 films of particles with different quantum dot sizes were prepared. A photo of a typical sample is given in Figure 3a. The UV−vis absorption was measured on all films, and normalized absorption data are given in Figure 2b. For direct semiconductors, like ZnO, the optical band gap, E_g, can be extracted by plotting the square of the absorption against photon energy. If the linear region, found for photon energies slightly above the band gap energy, is extrapolated to zero absorption, as in Figure 2c, the band gap is given as the intercept with the abscissa. The optical band gap increases for smaller particles while they are small enough to be in the optical quantum confined regime. For ZnO particles, this is the case while the particle diameter is below approximately 9 nm. In this region, the bulk band gap has to be modified to include the limited physical extension of the material. Using the effective mass approximation and a confinement model of particles in a spherical potential well, one obtains eq 9[17,34]
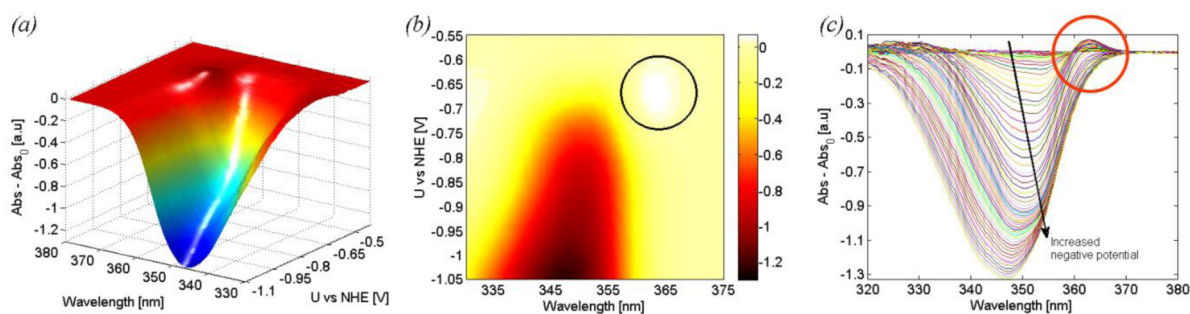
Figure 4. (a) Difference in absorption as a function of wavelength and applied potential for a representative sample with 6.2 nm particles. (b) The data in (a) represented as a couture plot. Marked by the black ring is a region with a positive value of the absorption difference. (c) Difference in absorption against wavelength for different applied potentials. Marked by the red ring is an increase in the absorption difference.
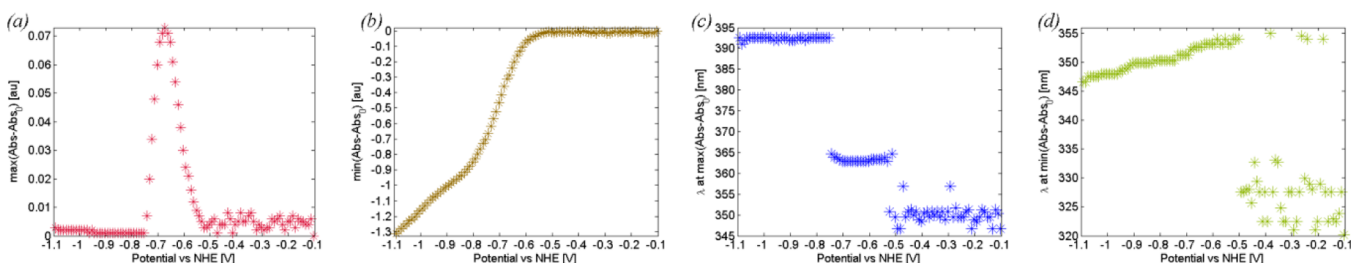

Figure 5. (a) Maximum value of the difference in absorption as a function of applied potential for the sample with 6.2 nm particles. (b) Minimum value of the difference in absorption as a function of applied potential. (c) The wavelength at which the maximum in (a) is occurring as a function of applied potential. (d) The wavelength at which the minimum in (b) is occurring as a function of applied potential.

$$E_g = E_{g,bulk} + \frac{\hbar^2 \pi^2}{2R^2}\left(\frac{1}{m_e^*} + \frac{1}{m_h^*}\right) - \frac{1.8e^2}{\varepsilon R}$$
$$+ \frac{e^2}{R}\sum_{n=1}^{\infty}\alpha_n\left(\frac{r_e + r_h}{R}\right)^{2n} \tag{9}$$

where E_g is the band gap of the bulk material, the second term is the increased kinetic energy caused by the localization of the electron−hole pair inside a sphere with radius R and scales as R^{-2}, the third term is the Coloumb attraction in a screened environment and scales as R^{-1}, and the fourth term is the average polarization of individual contributions α_n and also scales as R^{-1}. This gives a physical motivation for a functional dependence between the band gap, E_g, and the particle diameter, d, as $E_g = E_{g,bulk} + K_1/d + K_2/d^2$ where the constants K_1 and K_2 can be determined empirically.

Using a large number of samples, the band gap, given in eV, has empirically been related to the particle diameter, d, according to eq 10,[16] where the diameter is given in nanometers.

$$E_g = 3.30 + \frac{0.293}{d} + \frac{3.94}{d^2} \tag{10}$$

The volume-averaged particle sizes could thus be extracted from the optical data in Figure 2, and they span between 4.6 and 8.6 nm in diameter. The band gap and the particle sizes for all analyzed particles are given in Table S.1 of the Supporting Information.

The key measurements in this paper are the potential-dependent absorption measurements, which were performed on thin films of ZnO particles deposited on FTO. A photo of one of the ZnO films is shown in Figure 3a. The experimental setup is a conventional three-electrode measurements as illustrated in Figure 3b. The optical absorption of the films

was measured simultaneously as the potential over the film, with respect to the Ag/AgCl reference electrode, was scanned from −0.3 to −1.3 V. Potential-dependent absorption can also be used as a convenient method for determining the absolute energetic position of the band edges, which were described in a previous paper, and exemplified on these particles.[17]

Absorption against wavelength and applied potential is given for a representative sample with 6.2 nm particles in Figure 3c. All the data for a specific sample is given within the 3D surface, but to simplify the visible interpretation, the data is projected down to two dimensions as in Figure 3d. The full data set for all the analyzed particle films are given in the Supporting Information.

The property of primary interest here is not the absorption in itself, but rather the difference in absorption caused by the applied potential. This is given by subtracting the absorption for the film at its rest potential, when not connected to the potentiostat, from the absorption measured at each potential. The corresponding 3D surface, where the difference in absorption is plotted against wavelength and applied potential, is given for a representative sample in Figure 4a. Also here the data are projected down to two dimensions to simplify the readability. This is represented as a contour plot in Figure 4b and as the difference in absorption against wavelength for different potentials in Figure 4c.

The dominant feature in the measurements is a decrease in the absorption, once the potential is negative enough. This is completely in line with the model of the Burstein−Moss shift described previously[17] and also briefly outlined in the Theory section. A sufficiently negative potential will shift the Fermi level into the conduction band, whereupon states in the conduction band are filled by electrons and preventing excitation of electrons into these states. Important to remember is that the principle of charge neutrality requires a nearby positive charge to balance the negative electrons populating the
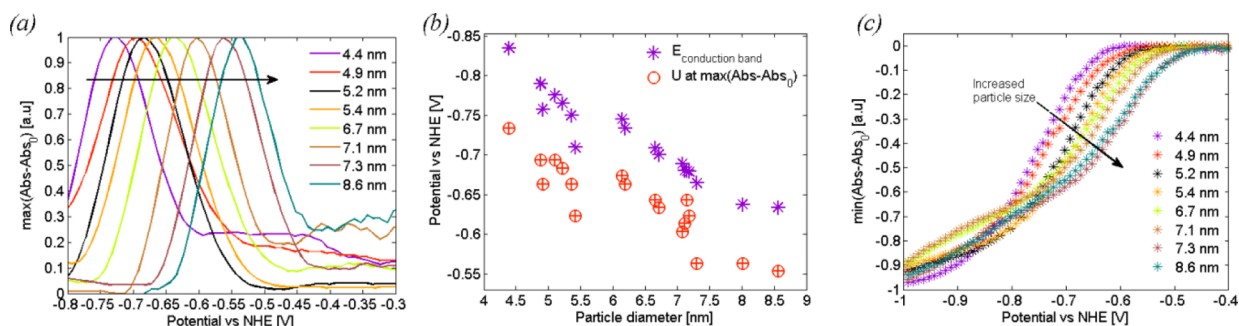
Figure 6. (a) Maximum value of the absorption difference as a function of applied potential for a subset of the analyzed samples. Data are normalized to ease the comparison. (b) Applied potential for the maximum of the maximum of the absorption difference as a function of particle size. This is compared to the position of the conduction band edge. (c) Minimum value of the absorption difference as a function of applied potential for a subset of the analyzed samples. Normalized data are used.
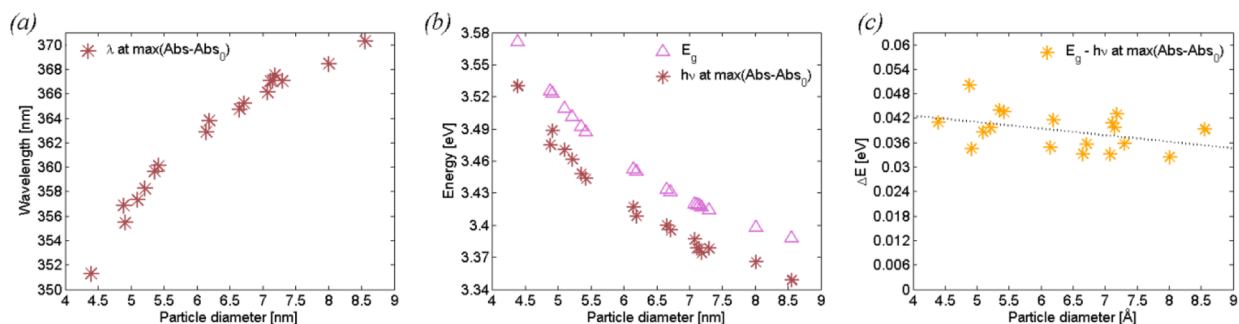

Figure 7. (a) Wavelength at the potential where the difference in absorption reaches its maximum as a function of particle size. (b) The corresponding photon energy and the band gap energy as a function of particle size. (c) Difference in energy between the band gap and the phonons corresponding to the maximum in the absorption difference.

conduction band. This is here supplied by counterions in the electrolyte. For the process to work there needs to be sufficiently large surface area to which the counterions can approach. Nanoporous films are thus required for this effect to be as pronounced as it is here. The decrease in absorption was described in detail in a previous paper where the band edge positions were determined[17] and will therefore not be the focus for the remainder of this paper.

The focus will instead be directed toward a smaller but opposite effect. In Figure 4, it is observed that the absorption actually increases somewhat for certain wavelengths before the potential is negative enough to cause a general absorption decrease. This shows that a more detailed description is needed in order to understand the nature of the states and the transition probabilities in the particles and that more than one effect influences the absorption under these circumstances.

In order to investigate this further, the value of the maximum in the absorption difference was plotted as a function of applied potential, as in Figure 5a. The increase in absorption is there seen to occur in a rather narrow potential interval of around 0.2 eV. The wavelength corresponding to the maximum in the absorption difference is given in Figure 5c and is observed to be rather constant within the 0.2 eV potential interval where the maximum in Figure 5a is located. Outside this interval, there is no distinct maximum of the absorption difference, and the values given outside the peak in Figure 5a are due to noise, reflected in the fact that the corresponding wavelengths in Figure 5c are either considerably higher or lower than at the maximum.

The minimum of the difference in absorption is plotted in an analogous way in Figure 5b. This value is close to zero until the

potential reaches a threshold, where after it decreases monotonically. There is, however, a distinct change in the slope at the potential where the increase in absorption difference ends. The wavelength corresponding to the minimum decreases monotonically, once the difference in absorption starts to decrease, as seen in Figure 5d.

The maximum for the maximum of the absorption difference in Figure 5a occurred at a distinct potential, but it turns out that the position of this maximum shifts to less negative potentials with increased particle sizes, as seen in Figure 6a. In Figure 6b, these values are compared to the potential corresponding to the conduction band positions, which were measured and discussed before.[17] The trends for the two values are nearly identical with respect to particle size, even though the maximum for the maximum of the absorption difference are located around 80 mV (mean 78 mV) below the conduction band edge, regardless of particle size.

Also, the minimum of the absorption difference (plotted in Figure 5b) shifts with respect to particle size, as seen in Figure 6c. The potential where the absorption starts to decrease follows the same trend with respect to particle size as the maximum does and is shifted to higher potentials for larger particles. The initial slope of the minimum in absorption difference with respect to potential is very similar for the different samples, but this slope decreases and starts to deviate more for lower potentials. The change in slope coincide with the potentials where there no longer is any maximum in the absorption difference.

It is thus reasonable to assume that the experimental behavior is the result of a combination of two effects. The dominant one is the decrease in absorption due to the band
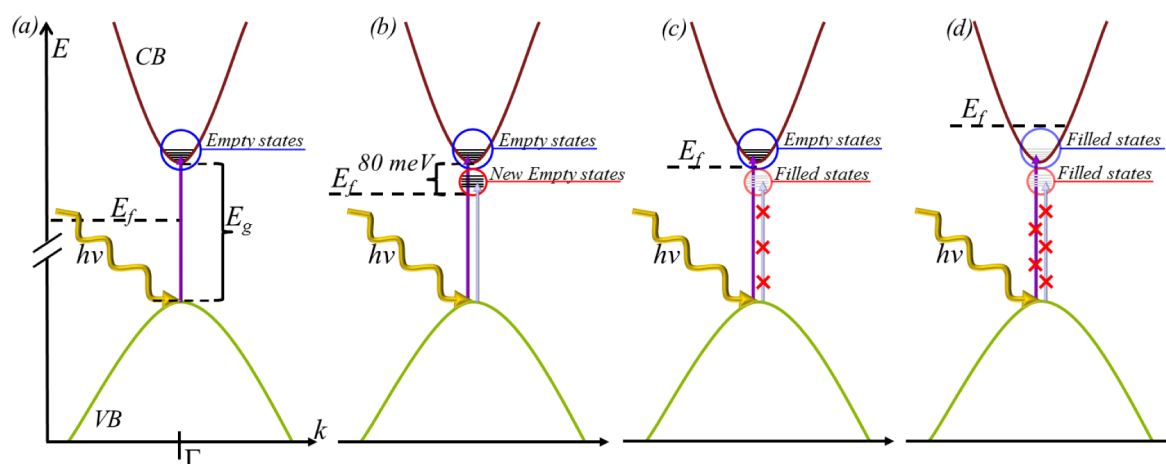
Figure 8. A graphical summary of the energy states involved in the observed absorption increase. (a) In the undisturbed case absorption is occurring from the bottom of the valence band to the conduction band. (b) When the applied potential reaches around 80 meV below the conduction band edge, new states are introduced in the band gap acting as acceptor states and increase absorption for certain wavelengths. (c) At even more negative potentials these states are filled with electrons from the potentiostat preventing them from acting as acceptor states in the absorption. (d) When the potential pushes the Fermi level into the conduction band, states in the conduction band gets populated by electrons from the potentiostat leading to a decreased absorption according to the Burstein−Moss effect.
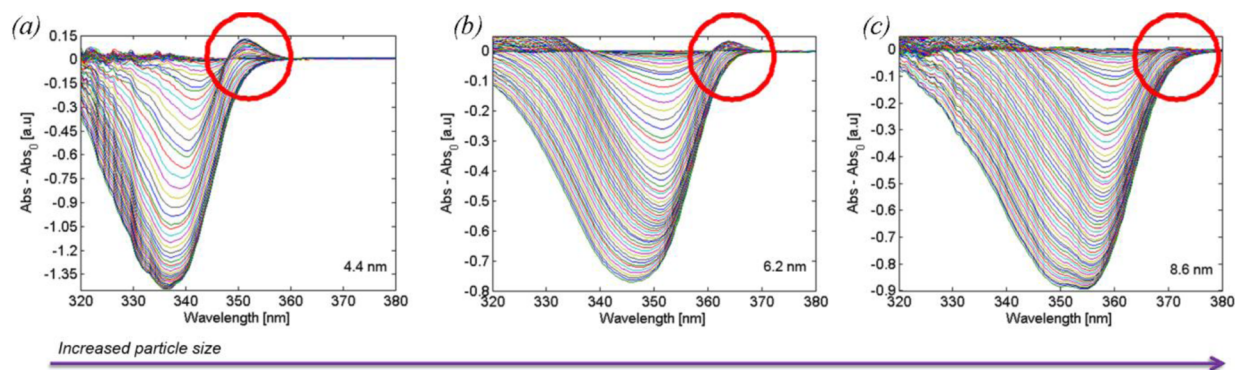

Figure 9. Difference in absorption plotted for different applied potentials. (a) For sample 1 corresponding to 4.4 nm particles. (b) For sample 9 corresponding to 6.2 nm particles. (c) For sample 18 corresponding to 8.6 nm particles. The full set of figures is given in the Supporting Information.

filling in accord with the potential analogue to the Burstein−Moss effect. Overlaid on this, in a potential interval of approximately 0.2 eV, is a smaller effect that causes the local absorption increase.

A question of interest is the energy of the photons absorbed causing the observed increase in absorption. In order to analyze this, the wavelength at the maximum of the absorption difference was extracted from Figure 5c. This wavelength is plotted as a function of particle diameter in Figure 7a and is in Figure 7b converted to photon energy and compared to the band gap energy. This photon energy follows the band gap energy smoothly with respect to particle size but is 40 meV smaller than the band gap energy, as seen in Figure 7c. The value is rather constant with respect to particle size, even if a small tendency of a trend toward smaller values with larger particles can be noticed in Figure 7c.

These data show that the absorption increase is caused by absorption to states within the band gap, located at least 40 meV below the conduction band edge. The peak value is likely caused by a transition from states slightly below the valence band edge to the center of distribution of these new states. The center position of the new states is thus probably located between 40 and 80 meV below the conduction band edge.

As this absorption is absent when no external potential is applied, it follows that these states are induced as a consequence of the applied negative potential. When the applied potential not is low enough, these states are not there, but when it reaches a value corresponding to around 80 meV below the conduction band edge, they begin to emerge and cause the observed increase in absorption. When the applied potential, and thus the Fermi level, is lowered even further, these states starts to be occupied with electrons from the potentiostat. Once occupied, they are no longer available as acceptor states in an absorption process, and no increase in absorption is seen. This explains why the absorption increase only is seen in a limited potential interval. A graphical summary of the findings so far is given in Figure 8, illustrating how new states in the band gap are created as the Fermi level rises, causing an increase in the absorption, where after they begin to be occupied and prevent a further absorption increase.

Interestingly, the magnitude of this effect turns out to be a function of particle size. The difference in absorption against wavelength for different applied potentials is given for three different particle sizes, ranging from the smallest to the largest in Figure 9. It can be observed that the effect of the local absorption increase, at moderate negative potentials, decreases as a function of particle size and essentially disappears for the

largest particles. In order to quantify this, the maximum of the difference in absorption, divided by the minimum of the absorption difference, is plotted as a function of particle size in Figure 10. This verify what is seen in the two-dimensional
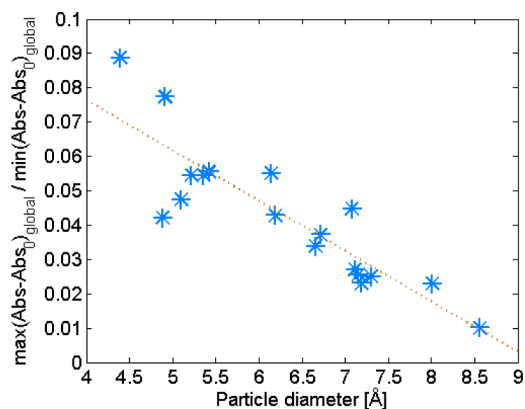

Figure 10. Maximum of the difference in absorption, divided by the minimum of the absorption difference, as a function of particle size.

projections in Figure 9. For the smallest particles, the magnitude of the absorption increase is up to 9% of the magnitude of the absorption decrease due to the Burstein–Moss effect, whereas it essentially disappears for particles approaching 9 nm.

One possible mechanism behind the introduction of states in the band gap is that the applied potential by the potentiostat will create an electric field within the ZnO particles, strong enough to cause a splitting of the existing energy levels. Once the potential from the potentiostat deviates from the electrochemical potential of the electrolyte, there will be a potential drop between the back contact of the electrode and the electrolyte. This will be portioned between the semiconductor and the double layer in the electrolyte. For a 100 nm thick film and assuming that half of the potential drop is occurring uniformly over the film, a potential difference of 0.1 V give rise to an electric field in the order of 5 kV/cm in the semiconductor. This is a rough order of magnitude estimate, and the local field can most likely be substantially different.

Under the influence of an external electric field, the band edge absorption is known to change in semiconductors, even if the amount of electrons not is changed as is the case of the potentiostatic control utilized above. This phenomenon can be described in terms of the Franz–Keldysh effect[35,36] and gives an exponential increase of the absorption for photon energies slightly below the band gap energy in a semiconductor with an electric field applied. For light with higher energy than the band edge, the absorption coefficient, within this framework, is modulated via an oscillatory function.[37,38] Adding an additional electron–hole interaction from the Coulomb field in the Schrödinger equation results in a uniform-field wave function giving an oscillatory behavior in the absorption at higher energy than the band gap.[39]

The Stark effect, which causes a splitting of the orbitals in the electric field, can be affected by quantum confinement because of potential barriers hindering full effects of the field. The effect of such an electric field for the oscillatory behavior in quantum wells has theoretically been studied in terms of a quantum confined Stark effect[40–42] and also been explored for theoretical models of ZnO dots and wires.[43,44] This gives a model for high

fields whereas the system studied here also have an electrolyte penetrating the electrode leading to a shielding. This implies a different situation and is also evident from the data from our system where no oscillatory absorption is seen above the band gap energy.

The local field strengths may, however, be high enough to split the energy levels in the conduction band. For atomic and molecular systems, this would correspond to the well-known Stark effect, where an external electric field can break symmetry and thereby splitting energy levels and pushing some of them up and other down in energy. In the case of semiconducting nanoparticle, this would correspond to a smearing out of the energy levels in the conduction band. Some of them would then be shifted down into the band gap where they could act as acceptor states for sub-band-gap absorption. This would be in line with the experimental observations.

In the case of nanoporous electrodes, the surface properties would also affect the absorption behavior. If the energy states introduced by the applied potential are associated with the particle surface, this could explain the decrease in absorption gain with increased particle size. While going from a 4.4 nm particle to a 8.6 nm particle, the volume to surface area ratio increases by a factor 1.8. This is smaller than the factor 8 that according to Figure 10 differs between the magnitude of the absorption gain compared to the absorption bleaching between the smallest and the largest particles. If the effective surface region extend a few layers within the particles, the trend in decreased absorption gain with increased particle size couples better with the decrease in active surface in the system. This does not pinpoint the cause of the absorption gain but indicates that it is reasonable to associate it with the surface. A possible mechanism behind introduction of states associated with the surface is reduction of the surface or species at the surface. While the potential is decreased, there is a cathodic current flowing through the film. In part, this has a capacitive origin, at least until the potential gets negative enough for water decomposition, but part of it is also faradaic. This could very well be a part of the cause of the introduction of new states in the band gap. It is also in line with the observed size dependence. As the optical effect is reversible with respect to potential, so must the possible redox reaction at the surface be.

Another possibility for the absorption increase is a stabilization of the exciton. The energy difference between the band gap and the photons absorbed, causing the local increase in absorption, is not very far from the exciton binding energy of around 60 meV. This is commonly seen at low temperature but not so far in steady-state absorption at room temperature. Recent ultrafast spectroscopy performed on ZnO quantum dots show 3 times longer exciton emission lifetime for smaller particles (<5.5 nm) compared to larger particles (>5.5 nm), suggesting a stabilization of excitons in the smaller particles.[45] A possibility is thus that the applied potential generate an electric field that stabilizes the excitons and more so for the smallest particles. To find more clues for the origin of the effect, transition probabilities to states slightly above the band gap are analyzed below.

Changes in the Absorption Coefficient. The absorption, A, for a direct semiconductor is for photon energies, $h\nu$, slightly above the band gap, E_g, given by eq 11, where α is the absorption coefficient, l the optical path length, and C_1 the effective absorption coefficient which includes the optical path length but not the energy scaling.
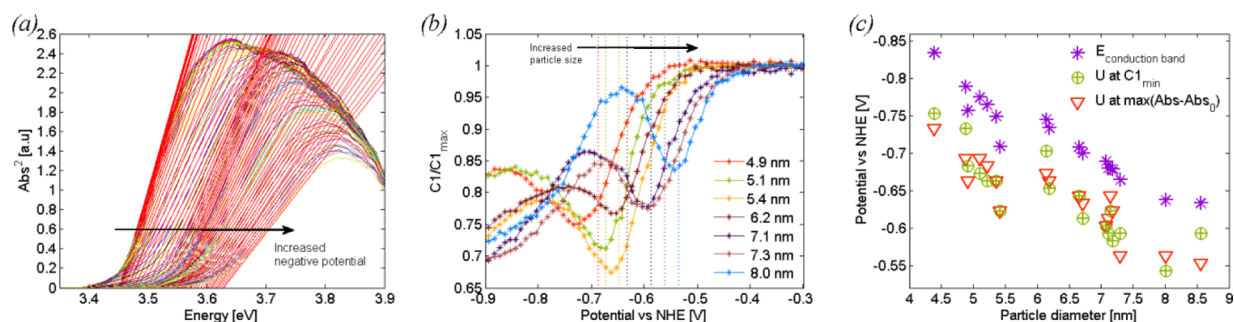
Figure 11. (a) Square of the absorption against photon energy for successively more negative applied potentials. The effective absorption coefficient C_1 is given by the slope of the red lines. (b) Effective absorption coefficient C_1 as a function of applied potential for a subset of the samples. Normalized data are used. (c) Comparison between the position of the conduction band edge and the applied potential for the maximum of the maximum of the absorption difference and the local minimum in C_1 as a function of particle size.

$$A = \alpha l = C_1(\hbar\omega - E_g)^{1/2} \qquad (11)$$

Conceptually, the absorption coefficient is simply the product of the number of accessible donor states, the number of accessible acceptor states, and the probability for a transition from one of the door states to one of the acceptor states. In eq 11, the energy scaling comes from the number of states given in the parabolic approximation and C_1 contains all other factors where C_1 can be identified from eq 7 to be

$$C_1 = \frac{2\mu_{vc}^2}{\pi m_v^* nc\varepsilon_0\omega}\left(\frac{2m_{red}^*}{\hbar^2}\right)^{3/2} \qquad (12)$$

If the square of the absorption is plotted against photon energy, as in Figure 2.c, the coefficient C_1 is readily extracted from the slope of the linear region. This analysis can easily be performed as a function of applied potential, as illustrated in Figure 11a. As shown in Figure 11b, the effective absorption coefficient is a function of the applied potential. While starting from more positive potential, and going toward more negative potentials, the value of C_1 is constant until it reaches the potential where the local absorption gain starts to be observed. After that, it decreases until it reaches a local minimum. At slightly more negative potentials, a local maximum is occurring where after the decrease continuous.

The position of the local minimum is shifted to less negative potentials with increased particle size. In Figure 11c, this value is compared to the band edge position and the potential corresponding to the position of the local absorption maximum. It turns out that the particle size dependence of the potential of the minimum in the absorption coefficient correlates well with the potential for the local absorption increase.

The dominating feature of the potential dependence of the effective absorption coefficient is a decrease with increased potential. There could be several mechanisms behind this, but the two most likely once are a decrease in the number of accessible acceptor states in the conduction band and a decrease in the transition probability. When the potential becomes more negative, a buildup of an electric field is expected within the particles. Such a field may increase the spatial separation of the excited electrons and holes. The orbital overlap between the electron and the hole wave functions would thus decrease and thus also decrease the transition probability between these states. This would then, in terms of eq 12, mean that the transition dipole moment between the two dominating states, μ_{vc}, decreases. A second effect can also

be expected with a shift in the number of accessible acceptor states in the conduction band, as some of the states are pushed down below the conduction band edge. As long as analysis of the absorption coefficients is made in between the valence band and conduction band states, the utilization of the equations should be valid. The absorption coefficient starts to decrease at the same potential as there starts to be an increase in the difference in absorption, as seen in Figure 12 where the
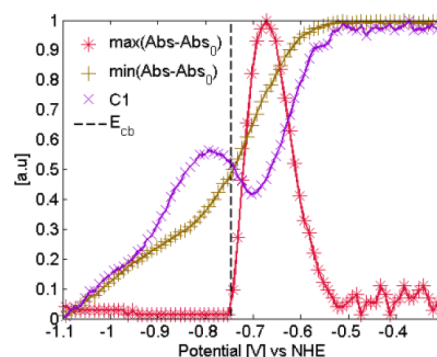

Figure 12. Comparison between the absorption increase, the absorption decrease and the effective absorption coefficient as a function of applied potential for the sample with 6.2 nm particles. Data are normalized to enable the comparison. The position of the conduction band edge is given as the vertical line.

different curves are compared directly. The new states introduced in the band gap at this potential increases the absorption for wavelengths with energy slightly lower than the band gap and is not reflected in the absorption coefficient, C_1, as it is only derived for transitions between valence and conduction band states. The decrease in C_1, however, indicates a decrease in the number of acceptor states as a function of applied potential, which then would mean that some of the density of states in the conduction band is shifted up in the conduction band and down into the band gap. This would be an explanation in line with the Stark effect. It is also in line with the fact that the potential for the maximum in the absorption increase coincide with the local minimum in the effective absorption coefficient.

After the potential is becoming more negative than the position of the band edge, C_1 continues to decrease, which would be due to filling of states in the conduction band from the potentiostat.

The first mechanism that comes to mind is that the field can penetrate the smaller particles, causing a Stark splitting of all the states in the particle, whereas the inner part of the larger particles have no effective Stark splitting. In Figure 11b one can see that the magnitude of the decrease of the absorption coefficient (for transitions to states above the conduction band edge) for 8 nm particles is approximately half of the decrease of the 5 nm particles. Densification of the orbitals for the largest quantum dots could possibly also effect the effective Stark splitting. As all particle sizes show a decrease of the absorption coefficient for transitions above the band gap energy when a potential corresponding to energies below the conduction band edge is applied (as evident from Figure 11b,c) they all are affected by the Stark effect. The Stark effect, however, is less effective for the largest particles but evidently still there.

The mechanism of the phenomena thus seems to be slightly more intricate than a total lack of Stark-induced states for the largest particles and also dependent on a change in transition probability to the induced states. If the system can be described with an effective wave function for the initial (i) and final states (f) for the induced states, analogous to eq 4, the probability for the sub-band-gap transition would be related to the transition dipole moment for the transition (μ_{if}) and thus the overlap of the wave functions. The size-dependent absorption into states induced below the conduction band edge can then be rationalized with a quantum confined Stark effect with two effects where (i) the Stark effect splitting is less effective for the largest particles as evident in Figure 11b and (ii) a decreased transition probability shown in Figure 9b that could originate in a decreased orbital overlap between the electron and the hole wave functions as the particles becomes larger. In small particles (~5 nm), the spatial confinement prevents the local electric field to effectively separate the electron and hole wave functions to decrease the transition dipole moment. In the larger particles (~9 nm), the field then seems to effectively separate the wave functions of the electron and hole. The two effects are schematically illustrated in Figure 13 below where the Stark splitting is illustrated as less effective for the inner part of the larger ZnO quantum dots but could also originate from more rigid and dense bands in the larger particles compared to the smaller particles.
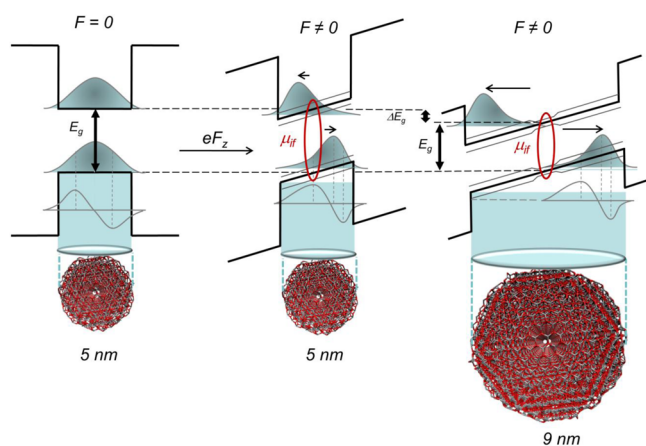

Figure 13. Schematic illustration of the quantum confined Stark effect, where the extension of the potential well limits the separation of the electron and effective wave functions for the electron and holes for the smallest particles and the Stark effect is less pronounced in the inner part of the largest particles in a field F.

Although other mechanisms can contribute to the effect, such as surface stabilized excitons in the smallest particles, the phenomenon can be rationalized by a quantum confined Stark effect and seems to be the most feasible mechanism from the data at this stage.

5. SUMMARY AND CONCLUSIONS

Thin films of ZnO quantum dots with 18 different diameters between 4 and 9 nm were investigated with photoelectrochemical methods. The optical absorption of these films have been measured as a function of applied potential, where the films were connected in an electrochemical three-electrode configuration and where the potential was controlled by a potentiostat. The dominant effect under such measurements is a decrease in the absorption due to potentiostatic filling of energy levels in the conduction band. This is a potentiostatic and electrochemical analogue to the Burstein–Moss effect for degenerate semiconductors. At Fermi levels before a Burstein–Moss bleach is seen, the absorption increased for wavelengths below the band gap energy in a limited potential interval of around 20 meV, centered 80 meV below the conduction band edge. This increase in absorption was caused by photons with energy centered 40 meV smaller than the band-gap energy. From this, the conclusion could be drawn that this absorption is caused by states within the band gap, located slightly below the conduction band edge, not present in the undisturbed case but instead induced as a consequence of the applied potential.

The phenomenon is analyzed in terms of the Stark effect, leading to a splitting of the energy states in the conduction band. Some of the energy states in the conduction band would consequently be shifted up in energy, whereas others would be shifted down into the band gap. The effect was quantified by the effective absorption coefficient, describing the absorption for photons of energies over the band gap, which was decreasing with more negative potential.

We also demonstrate that the optical absorption into the induced states is strongly dependent on particle size. For the smallest particles, which are 4.4 nm in diameter, the magnitude of the absorption gain is almost 10% compared to the absorption bleaching caused by the Burstein–Moss effect. For the largest particles, which are 8.6 nm and at the limit of being optically quantum confined, the magnitude of the absorption gain essentially disappears. All films with ZnO quantum dots showed a shift of orbitals as a result of applied potential and thus a Stark effect as probed by the decreased absorption for photon energies above the band gap, whereas transition probabilities to the induced states decrease with increase of particle size.

Possible reasons for these effects are discussed where the most feasible mechanism was found to be a quantum confined Stark effect with (i) a less effective Stark splitting of states for the larger particles and (ii) a decreased transition probability that could originate in a decreased overlap between the electron and hole wave function as the quantum dots are getting larger.

To further analyze the size-dependent nature of the induced states, and whether or not it could be of any technological use, will be the scope of future work.

■ ASSOCIATED CONTENT

Ⓢ Supporting Information

Supplementary mathematics and the full set of figures corresponding to absorption data in Figure 3c; differential absorption in Figure 4c; differential absorption maximum in

Figure 5a; differential absorption minimum in Figure 5b; potential at which the difference in absorption has its maximum as a function with particle size; difference between potential at maximum absorption and conduction band edge; a non-normalized version of Figure 6c; a version of Figure 10 but with global maximum compare to the minimum at exactly that potential; all the subplots for Figure 11b. This material is available free of charge via the Internet at http://pubs.acs.org.

■ AUTHOR INFORMATION

Corresponding Author

*E-mail tomas.edvinsson@kemi.uu.se; Ph +46 (0)18 471 3772 (T.E.).

Notes

The authors declare no competing financial interest.

■ ACKNOWLEDGMENTS

■ REFERENCES

(1) Serpone, N.; Dondi, D.; Albini, A. Inorganic and Organic UV filters: Their Role and Efficacy in Sunscreens and Suncare Product. *Inorg. Chim. Acta* **2007**, *360*, 794−802.

(2) Chae, D. W.; Kim, B. C. Characterization on Polystyrene/Zinc Oxide Nanocomposites Prepared From Solution Mixing. *Polym. Adv. Technol.* **2005**, *16*, 846−850.

(3) Heideman, G.; Datta, R. N.; Noordermeer, J. W. M.; van Baarle, B. Influence of Zinc Oxide during Different Stages of Sulfur Vulcanization. Elucidated by Model Compound Studies. *J. Appl. Polym. Sci.* **2005**, *95*, 1388−1404.

(4) Ekambaram, S. Combustion Synthesis and Characterization of New Class of ZnO-Based Ceramic Pigments. *J. Alloys Compd.* **2005**, *390*, L4−L6.

(5) Brown, K. H.; Wessells, K. R.; Hess, S. Y. Zinc Bioavailability from Zinc-Fortified Foods. *Int. J. Vitam. Nutr. Res.* **2007**, *77*, 174−181.

(6) Tang, Z. K.; Wong, G. K. L.; Yu, P.; Kawasaki, M.; Ohtomo, A.; Koinuma, H.; Segawa, Y. Room-Temperature Ultraviolet Laser Emission from Self-Assembled ZnO Microcrystallite Thin Films. *Appl. Phys. Lett.* **1998**, *72*, 3270−3272.

(7) Tsukazaki, A.; Ohtomo, A.; Onuma, T.; Ohtani, M.; Makino, T.; Sumiya, M.; Ohtani, K.; Chichibu, S. F.; Fuke, S.; Segawa, Y.; Ohno, H.; Koinuma, H.; Kawasaki, M. Repeated Temperature Modulation Epitaxy for p-Type Doping and Light-Emitting Diode Based on ZnO. *Nat. Mater.* **2005**, *4*, 42−46.

(8) Lee, C. J.; Lee, T. J.; Lyu, S. C.; Zhang, Y.; Ruh, H.; Lee, H. J. Field Emission from Well-Aligned Zinc Oxide Nanowires Grown at Low Temperature. *Appl. Phys. Lett.* **2002**, *81*, 3648−3650.

(9) Zhu, G. A.; Yang, R. S.; Wang, S. H.; Wang, Z. L. Flexible High-Output Nanogenerator Based on Lateral ZnO Nanowire Array. *Nano Lett.* **2010**, *10*, 3151−3155.

(10) Sharma, P.; Gupta, A.; Owens, F. J.; Inoue, A.; Rao, K. V. Room Temperature Spintronic Material - Mn-Doped ZnO Revisited. *J. Magn. Magn. Mater.* **2004**, *282*, 115−121.

(11) Wang, J. X.; Sun, X. W.; Yang, Y.; Huang, H.; Lee, Y. C.; Tan, O. K.; Vayssieres, L. Hydrothermally Grown Oriented ZnO Nanorod Arrays for Gas Sensing Applications. *Nanotechnology* **2006**, *17*, 4995−4998.

(12) Martinez, M. A.; Herrero, J.; Gutierrez, M. T. Deposition of Transparent and Conductive Al-Doped ZnO Thin Films for Photovoltaic Solar Cells. *Sol. Energy Mater. Sol. Cells* **1997**, *45*, 75−86.

(13) Wang, Z. L. Towards Self-Powered Nanosystems: From Nanogenerators to Nanopiezotronics. *Adv. Funct. Mater.* **2008**, *18*, 3553−3567.

(14) Quintana, M.; Edvinsson, T.; Hagfeldt, A.; Boschloo, G. Comparison of Dye-Sensitized ZnO and TiO$_2$ Solar Cells: Studies of Charge Transport and Carrier Lifetime. *J. Phys. Chem. C* **2007**, *111*, 1035−1041.

(15) Jacobsson, T. J.; Edvinsson, T. Antireflective Coatings of ZnO Quantum Dots and Their Photocatalytic Activity. *RSC Adv.* **2012**, *2*, 10298−10305.

(16) Jacobsson, T. J.; Edvinsson, T. Absorption and Fluorescence Spectroscopy of Growing ZnO Quantum Dots: Size and Band Gap Correlation and Evidence of Mobile Trap States. *Inorg. Chem.* **2011**, *50*, 9578−9586.

(17) Jacobsson, T. J.; Edvinsson, T. Photoelectrochemical Determination of the Absolute Band Edge Positions as a Function of Particle Size for ZnO Quantum Dots. *J. Phys. Chem. C* **2012**, *116*, 15692−15701.

(18) Jacobsson, T. J.; Edvinsson, T. A Spectroelectrochemical Method for Locating Fluorescence Trap States in Nanoparticles and Quantum Dots. *J. Phys. Chem. C* **2013**, *117*, 5497−5504.

(19) Hall, L. H.; Bardeen, J.; Blatt, F. J. Infrared Absorption Spectrum of Germanium. *Phys. Rev.* **1954**, *95*, 559−560.

(20) Fondell, M.; Jacobsson, T. J.; Boman, M.; Edvinsson, T. Optical Quantum Confinement in Low Dimensional Hematite. *J. Mater. Chem. A* **2014**, *2*, 3352−3363.

(21) Bardeen, J.; Blatt, F. J.; Hall, L. H. *Photoconductivity Conference, Atlantic City, 1954*; Wiley: New York, 1956.

(22) Fan, H. Y.; Sheperd, M. L.; Spitzer, W. *Photoconductivity Conference, Atlantic City, 1954*; Wiley: New York, 1956.

(23) Fan, H. Y. Infra-red Absorption in Semiconductors. *Rep. Prog. Phys.* **1956**, *19*, 107−155.

(24) Marton, L. *Advances in Electronics and Electron Physics*; Academic Press: New York, 1959; Vol. *VII*.

(25) Moss, T. S. *Optical Properties of Semi-Conductors*. Butterworths Sci. Pub.: Belfast, 1959.

(26) Pankove, J. I. *Optical Processes in Semiconductors*. Dover: Mineola, NY, 1975.

(27) Jackson, J. D. *Classical Electrodynamics*, 3rd ed.; Wiley: New York, 1998.

(28) Burstein, E. Anomalous Optical Absorption Limit in InSb. *Phys. Rev.* **1954**, *93*, 632−633.

(29) Moss, T. S. The Interpretation of the Properties of Indium Antimonide. *Proc. Phys. Soc. London, B* **1954**, *67*, 775−782.

(30) Meulenkamp, E. A. Synthesis and Growth of ZnO Nano-particles. *J. Phys. Chem. B* **1998**, *102*, 5566−5572.

(31) Spanhel, L. Colloidal ZnO Nanostructures and Functional Coatings: A Survey. *J. Sol-Gel Sci. Technol.* **2006**, *39*, 7−24.

(32) McMurdie, H. F.; Morris, M. C.; Evans, E. H.; Paretzkin, B.; Wong-Ng, W. Methods of Producing Standard X-Ray Diffraction Powder Patterns. *Powder Diffr.* **1986**, *1*, 40−43.

(33) Raymand, D.; Jacobsson, T. J.; Hermansson, K.; Edvinsson, T. Investigation of Vibrational Modes and Phonon Density of States in ZnO Quantum Dots. *J. Phys. Chem. C* **2012**, *116*, 6893−6901.

(34) Brus, L. E. Electron Electron and Electron-Hole Interactions in Small Semiconductor Crystallites - The Size Dependence of the Lowest Excited Electronic State. *J. Chem. Phys.* **1984**, *80*, 4403−4409.

(35) Franz, W. Einfluss Eines Elektrischen Feldes Auf Eine Optische Absorptionkante. *Z. Naturforsch., A* **1958**, *13*, 484−489.

(36) Keldysh, L. V. The Effect of a Strong Electric Field on the Optical Properties of Insulating Crystals. *Sov. Phys. JETP* **1958**, *7*, 788−790.

(37) Cardona, M.; Shaklee, K. L.; Pollak, F. H. Electroreflectance at a Semiconductor-Electrolyte Interface. *Phys. Rev.* **1967**, *154*, 696−720.

(38) Aspnes, D. E. Electric-Field Effects on Optical Absorption Near Thresholds in Solids. *Phys. Rev.* **1966**, *147*, 554−566.

(39) Dow, J. D.; Lao, B. Y.; Newman, S. A. Differential Electroabsorption. *Phys. Rev. B* **1971**, *3*, 2571−2581.

(40) Miller, D. A. B.; Chemla, D. S.; Damen, T. C.; Gossard, A. C.; Wiegmann, W.; Wood, T. H.; Burrus, C. A. Band-Edge Electroabsorption in Quantum Well Structures: The Quantum-Confined Stark Effect. *Phys. Rev. Lett.* **1984**, *53*, 2173−2176.

(41) Brum, J. A.; Bastard, G. Electric-Field-Induced Dissociation of Excitons in Semiconductor Quantum Wells. *Phys. Rev. B* **1985**, *31*, 3893−3898.

(42) Miller, D. A. B.; Chemla, D. S.; Damen, T. C.; Gossard, A. C.; Wiegmann, W.; Wood, T. H.; Burrus, C. A. Electric Field Dependence of Optical Absorption Near the Band Gap of Quantum-Well Structures. *Phys. Rev. B* **1985**, *32*, 1043−1060.

(43) Congxin, X.; Spector, H. N. Confined Franz-Keldysh Effect in ZnO Quantum Dots. *Superlattices Microstruct.* **2010**, *47*, 490−495.

(44) Xia, C. X.; Wei, S. Y.; Spector, H. N. Franz-Keldysh Effect in ZnO Quantum Wire. *Physica E* **2010**, *42*, 2065−2068.

(45) Jacobsson, T. J.; Viarbitskaya, S.; Mukhtar, E.; Edvinsson, T. A Size Dependent Discontinuous Decay Rate For the Exciton Emission in ZnO Quantum Dots. *Phys. Chem. Chem. Phys.* **2014**, DOI: 10.1039/C4CP00254G.